# Electronic and lattice excitations in $BaTiO_3$:La



1994 J. Phys.: Condens. Matter 6 10159

(http://iopscience.iop.org/0953-8984/6/46/031)

J. Phys.: Condens. Matter 6 (1994) 10159–10170. Printed in the UK

# Electronic and lattice excitations in $BaTiO_3$:La

M Kchikech and M Maglione

Laboratoire de Physique, Université de Bourgogne, BP 138, 21004 Dijon, France

Received 7 March 1994, in final form 19 July 1994

**Abstract.** We report lattice and electronical properties of $BaTiO_3$:La powders and ceramics with $0 < x_{La} < 20$ at.%. Dielectric measurements and x-ray scattering evidence a continuous decrease of the ferroelectric transition temperature when the La content is increased. For $x_{La} = 20$ at.%, no dielectric maximum is found for temperatures higher than 20 K. At the same time, an impurity mode at 840 $cm^{-1}$ increases linearly with $x_{La}$. We have modelled these data using a linear chain model with one polarizable ion. The electric excitations were probed using DC conductivity, EPR spectroscopy and optical absorption. This last technique was applied to $BaTiO_3$:La single crystals, which were grown for the first time in our laboratory. Our main result is that the conductivity maximum at $x_{La} \approx 0.5$ at.% is related to an impurity level lying 2.1 eV below the conduction band.

## 1. Introduction

$BaTiO_3$:La ceramics are commonly used in varistor devices because they display a strong PTCR (positive temperature coefficient of resistivity) effect for $x_{La} \approx 0.5$ % [1]. This effect is usually ascribed to the occurrence of grain boundary layers, which are strongly affected by the bulk cubic to tetragonal phase transition at 130 °C [2].

For a long time, interest was focused on this PTCR and not on the bulk properties of the mixed $BaTiO_3$:La system. Only recently was the ferroelectric phase diagram of this compound derived on the basis of dielectric and x-ray data [3]. The ferroelectric transition temperature was shown to decrease for $0 < x_{La} < 5$ at.% with increasing La content $x_{La}$. It is interesting to note that this behaviour had already been found some time ago in the parent system $PbTiO_3$:La [4].

It is the purpose of this paper to extend this previous study to higher La concentrations. Moreover, it was desirable to link the lattice properties of $BaTiO_3$:La to its peculiar conductivity.

To this end, we have performed x-ray, dielectric and Raman experiments in $BaTiO_3$:La up to $x_{La} = 20$ at.% and for temperatures 10 K $< T <$ 1000 K. At the same time, we investigated the electronic excitations in the same powered samples. This was achieved using conductivity and EPR data. We also report optical absorption spectra of $BaTiO_3$:La single crystals with $x_{La} < 1$ at.%. In the whole data set now available, it appears that the heterovalent substitution $La^{3+}/Ba^{2+}$ results in a non-monotonic perturbation of the lattice and electronic properties.

0953-8984/94/4610159+12$19.50  

## 2. Experiments

The $BaTiO_3$ powders and ceramics were processed in the standard solid–solid reactions [5]. La was substituted following the equation

$$La_2O_3 + 2TiO_2 \rightarrow 2La_{Ba} + 2e + 2Ti^{x}_{Ti} + 6O^{x}_{O} + \tfrac{1}{2}O_2.$$

The powders were pressed as rods using a isostatic process at 3 kbar. The sintering temperature was between 1300 °C and 1350 °C depending on the La content of the ceramics.

The resulting chemical formula is twofold:

(i) in the low-concentration limit $x_{La} < 0.5$ at.%, the electrical compensation of the heterovalent substitution is achieved through a Ti ionization [6]

$$Ba^{2+}_{(1-x)}La^{3+}_{x}\left(Ti^{4+}_{(1-x)}Ti^{3+}_{x}\right)O_3$$

(ii) in the high-concentration range $x_{La} > 0.5$ at.%, it is the $Ba^{2+}$ vacancies that play the dominant role [7]

$$La_2O_3 \rightarrow 2La_{Ba} + V''_{Ba} + O^{x}_{O} + \tfrac{1}{2}O_2.$$

These two compensation regimes are also found in the compound $PbTiO_3$:La [4]. Thus, the crossover concentration $x_{La} = 0.5$ at.% is already a crucial point for the chemical bonding in $BaTiO_3$:La. From the ceramics, a number of samples were cut, polished and electroded for Raman and dielectric experiments. These ceramics were milled to provide powders for x-ray and EPR experiments. From x-ray diffraction data, we verified that the crystallization was always higher than 99%.

The parameters of each of these experiments are reported in table 1.

**Table 1.** The experimental set-up and parameters used in this study. All the experiments were carried out on the same samples.

| Experiment | Sample processing | Temperature range | Frequency range wavelength |
|---|---|---|---|
| x-ray | powders | room temperature | Cu (K$\alpha$) |
| EPR | powders | 100 K $< T <$ 300 K | 9.5 GHz |
| Dielectric | Au electroded discs | 10 K $< T <$ 1000 K | 10 Hz $< f <$ $10^9$ Hz |
| Raman | polished discs | 100 K $< T >$ 300 K | 2 $cm^{-1} < f <$ 1000 $cm^{-1}$ |
| Optical absorption | single-crystal plate | room temperature | 300 nm $< \lambda <$ 900 nm |

Using a floating zone oven, some $BaTiO_3$:La ceramic rods were crystallized in a single-pass procedure [8]. In the low-concentration limit $x_{La} < 1$ at.%, single crystals were obtained. A preliminary neutron scattering experiment successfully probed a 1 $cm^3$ crystallized crystal. The density of defects was low enough to enable optical absorption experiments. To our knowledge, it is the first time that such data have been reported.

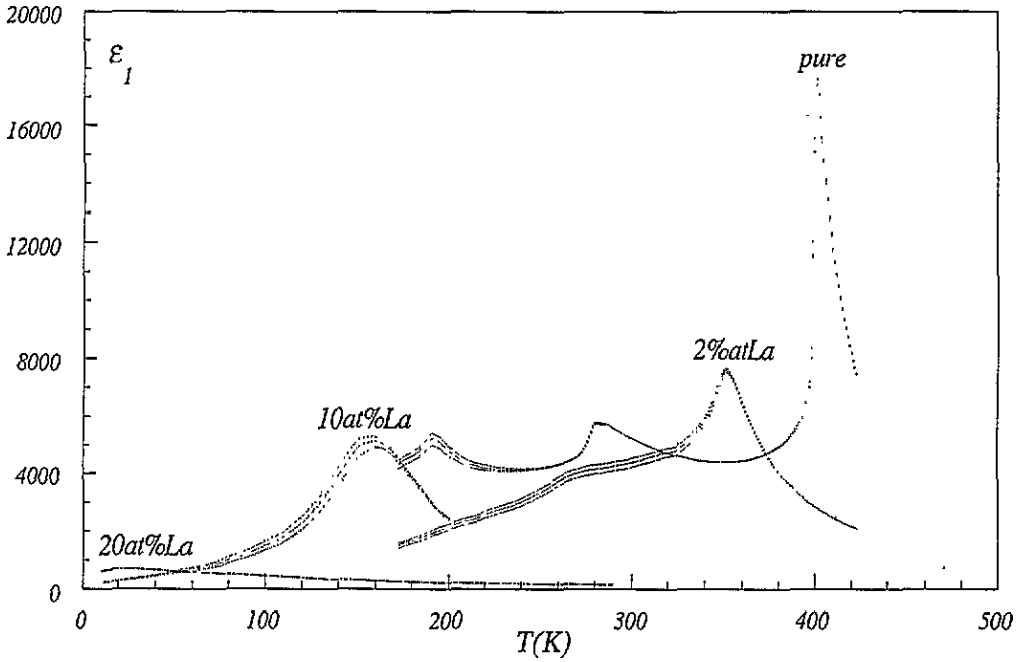


**Figure 1.** The temperature dependence of the low-frequency dielectric susceptibility of $BaTiO_3$ pure and La doped. The three operating frequencies were 1, 10 and 100 kHz.

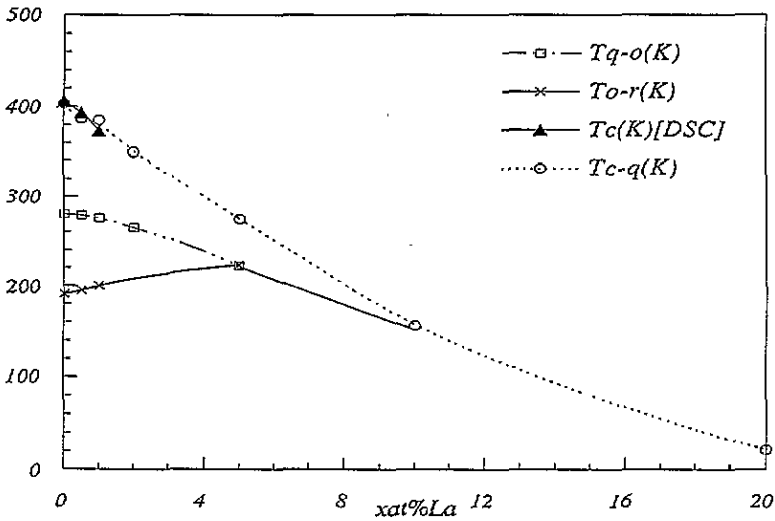


**Figure 2.** The ferroelectric diagram of $BaTiO_3$:La. The transition temperatures were obtained from dielectric measurements. Note the agreement with DSC experiments.

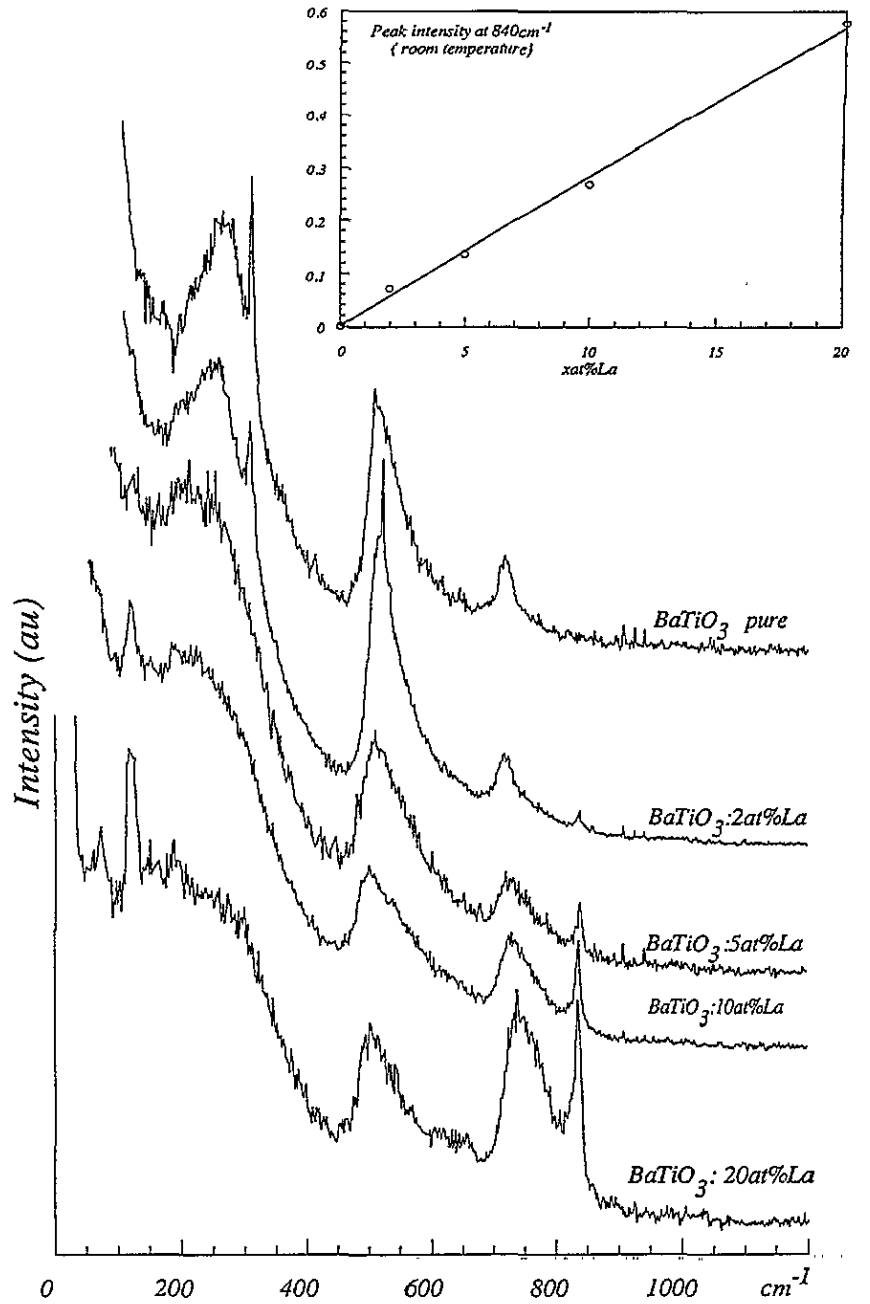


**Figure 3.** The effects of La substitution, at room temperature, on the $BaTiO_3$ Raman spectra. We report in the inset the peak intensity at 840 $cm^{-1}$ versus La content.

## 3. Results

We first report the ferroelectric properties of $BaTiO_3$:La for $x_{La} \leqslant 20$ at.%. In figure 1, the dielectric susceptibility is plotted as a function of temperature for several impurity

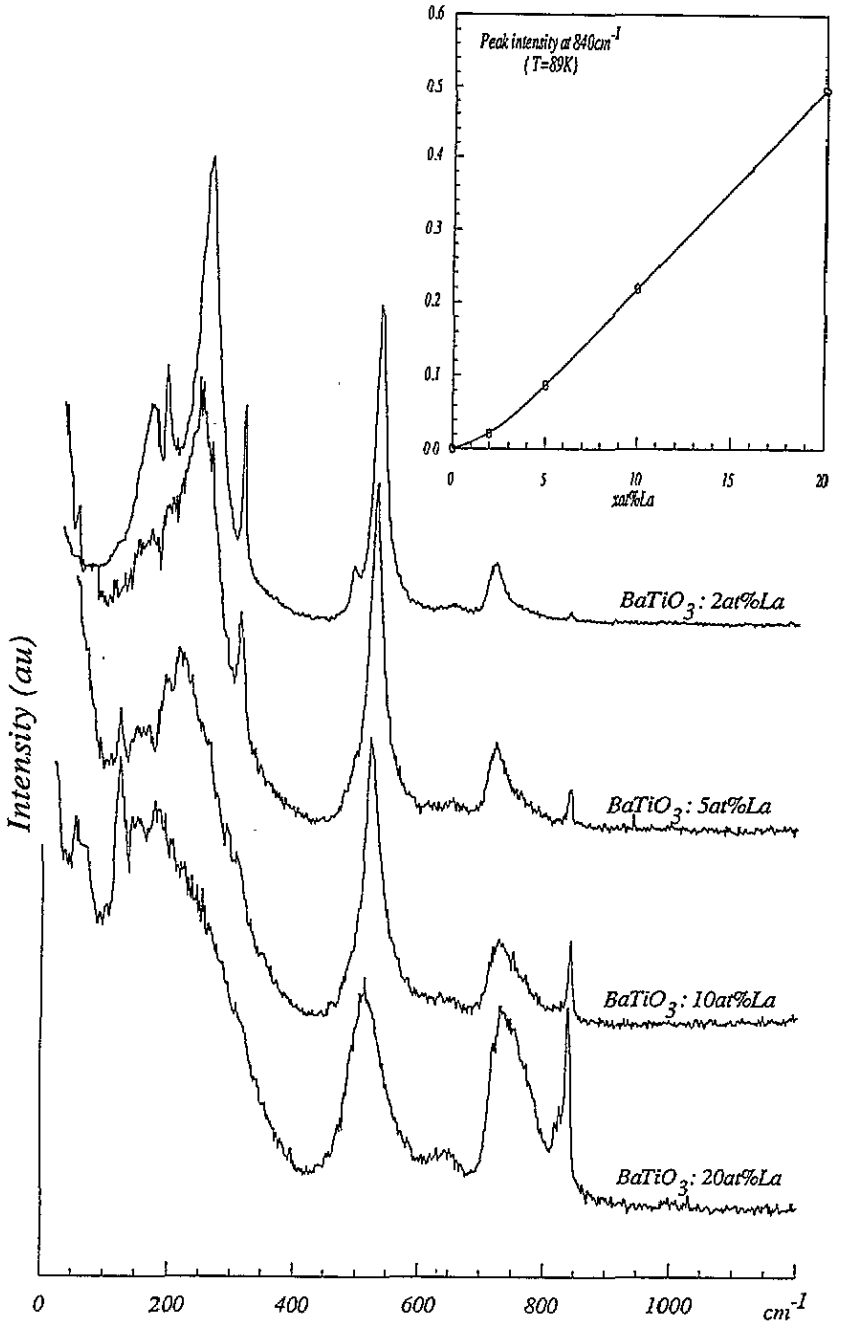


**Figure 4.** The same as figure 3 for $T = 89$ K.

contents. Up to $10^7$ Hz, no dielectric dispersion was found, which is proof of good sample homogeneity. The ferroelectric anomalies found on the $\varepsilon_1(T)$ curves continuously decrease when the La content increases. The transition temperatures are plotted in figure 2 versus the La content. It appears that the first ferroelectric transition temperature decreases

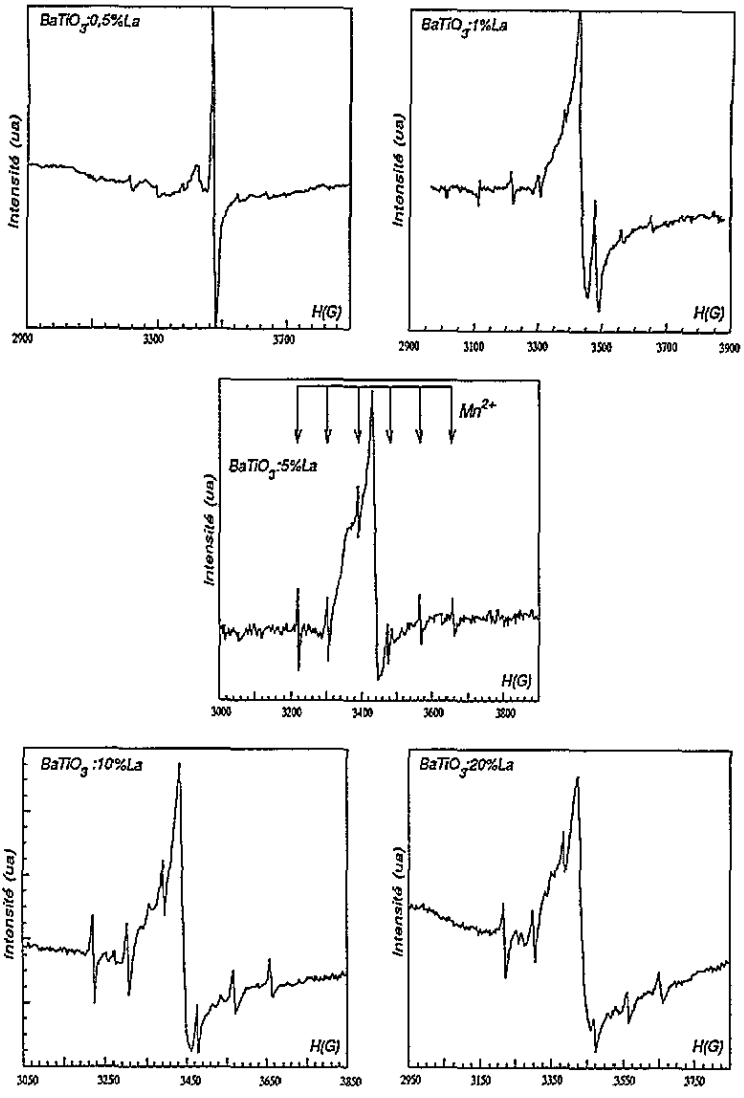


**Figure 5.** EPR spectra, at room temperature, for several $BaTiO_3$:La powders. The sextuplet is characteristic of the $Mn^{2+}$ ion.

continuously in agreement with similar data reported for $PbTiO_3$:La [4]. The intermediate tetragonal–orthorhombic and orthorhombic–rhombohedral transition lines disappear for $x_{La} > 5$ at.%. In figure 2, we have also plotted the transition temperature deduced from DSC measurements for the lowest La contents. In agreement with this ferroelectric diagram, we found, from x-ray data, that the $BaTiO_3$:La system is cubic at room temperature for $x_{La} \geqslant 5$ at.%.

A complete description of the lattice dynamical properties requires a Raman analysis. This is summarized in figures 3 and 4 where the Raman spectra of several $BaTiO_3$:La samples are reported at room temperature and at 89 K, respectively. In this temperature range the two sets of spectra are qualitatively the same: the Raman spectrum of pure $BaTiO_3$ is perturbed only at high frequencies. The 720 $cm^{-1}$ $A_1(LO_3)$ peak observed in

$BaTiO_3$ increases drastically when La is introduced into the lattice. Moreover, an 840 $cm^{-1}$ peak, which is not observed in pure $BaTiO_3$, appears in $BaTiO_3$:La ($x_{La}$ = 2 at.%) and increases with the La content. Such extra peaks are usually ascribed to impurity modes related to the pure lattice mode. However, the ionic mass ration $m_{La}/m_{Ba}$ = 1.0114 alone cannot account for the 840 $cm^{-1}$ line. In the insets of figures 3 and 4, the linear increase of these peaks versus the La content is displayed. There is thus a qualitative link between this linear variation and the monotonic decrease of the Curie temperature.

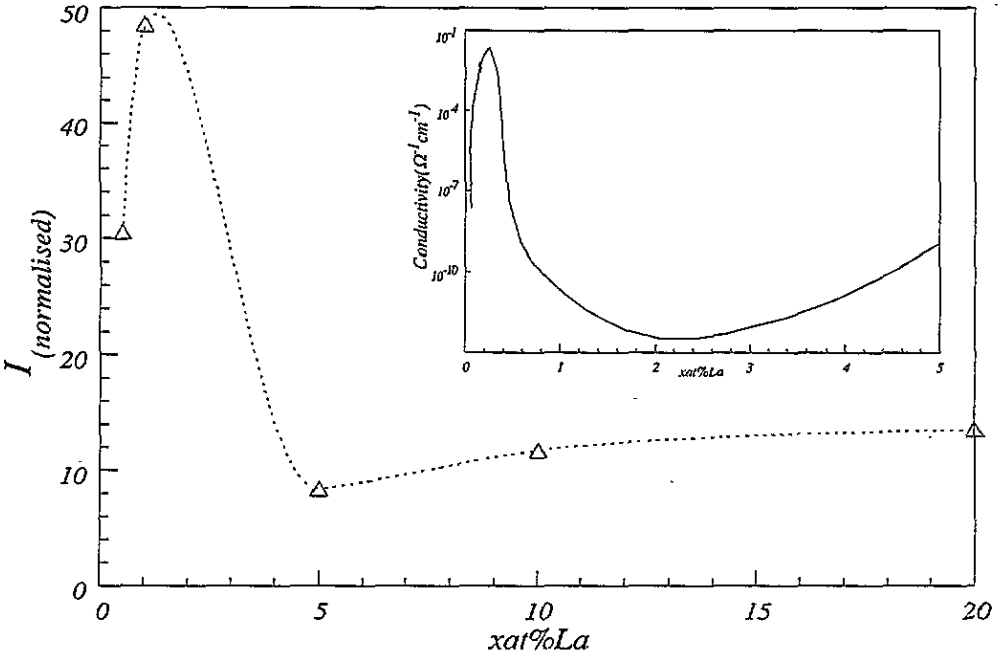


**Figure 6.** The central peak intensity versus La content deduced from EPR spectra a room temperature. In the inset, the effect of La on the conductivity in doped ceramics at room temperature is recalled [3].

We now investigate the electronic properties of $BaTiO_3$:La. EPR powder spectra were recorded at room temperature for all the La contents (figure 5). The six small lines result from $Mn^{2+}$ residual impurities with a factor $g$ = 1.992. We note that the signal to noise ratio of these lines is independent of the La content.

In contrast, the central line with a factor $g$ = 1.994 is very sensitive to this dopant. It is not possible to clearly ascribe this central line to a given centre. In fact, a great number of ions have a $g$ factor close to two such as $Ba^{2+}$ vacancies ($g$ = 2 [9]) or $Fe^{3+}$ centres ($g$ = 2.004 [10]). We also note that this central line can hardly be ascribed to $Ti^{3+}$ levels. In fact, this centre is usually not detected at room temperature due to its very high spin lattice relaxation time. At liquid helium temperatures, $Ti^{3+}$ centres with a $g$ factor of 1.934 were evidenced [11]. Keeping in mind this uncertainty regarding the exact origin of the central line, we can investigate its behaviour when the La content is raised. It is usually not easy to compare quantitatively EPR intensities in several samples. This is mainly due to the volume and granulometry of the powders, which are not reproducible. To overcome this difficulty,

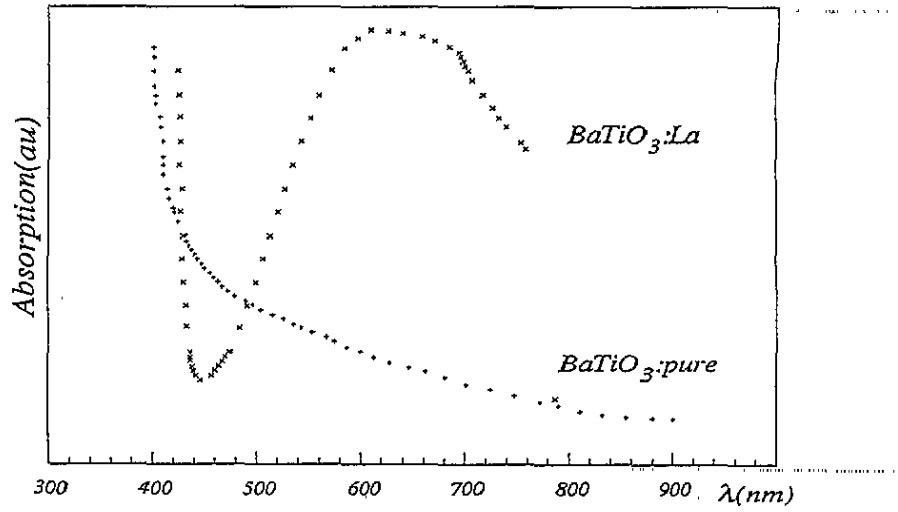


**Figure 7.** The absorption spectrum, in the visible range, of a $BaTiO_3$:La single crystal, at room temperature, compared to pure $BaTiO_3$.

we plotted in figure 6 the central line intensity normalized to the $Mn^{2+}$ line intensities. In fact these latter intensities are constant for all the $BaTiO_3$:La powders that we tested. This normalized intensity is a maximum for 0.5 at.% $< x_{La} <$ 1 at.%, and decreases for higher contents. This plot can be qualitatively compared to the room temperature conductivity of $BaTiO_3$:La (inset to figure 6 [3]). There is thus a similar evolution of microscopic EPR data and macroscopic conductivity results.

Optical absorption is usually performed in order to find the characteristic excitation energy of impurity centres in $BaTiO_3$. However, until now, no transparent $BaTiO_3$:La samples were available. The optical quality of some $BaTiO_3$:La samples ($x_{La} <$ 1 at.%) was good enough for optical absorption experiments. In figure 7, the broad absorption band of this sample is centred at 620 nm, which means that the absorbing levels are located 2.1 eV below the conduction band of $BaTiO_3$. Such an activation energy is commonly found in pure and doped $BaTiO_3$ [12]. From optical absorption on pulled single crystals these deep levels were ascribed to the $V_0^{00}/V_0^0$ ionization of O vacancies. It is somewhat surprising that these levels provide the maximum absorption in $BaTiO_3$:La. In fact, the electronic levels ($Ti^{3+}$, $V_0^{00}/V_0^0$) held responsible for the PTCR effect in $BaTiO_3$:La ceramics are close to the conduction band [2]. Moreover, the creation of O vacancies is not the predominant compensation mechanism for the $La^{3+}/Ba^{2+}$ substitution. Since it was not possible to grow single crystals with different dopant concentrations, we cannot describe these optical absorption data as we did for EPR spectra. It is thus not possible to confirm the maximum EPR intensity for $x_{La} \approx 0.5$ at.% by optical means.

To summarize, the possible link between the lattice dynamics and the conductivity properties is not clear at the experimental level.

## 4. Discussion

We first try to extract some microscopic information from the lattice dynamics of $BaTiO_3$:La. We already pointed out that a simple mass effect is to be excluded to account for the peculiar

Raman spectrum of $BaTiO_3$:La. Thus, the heterovalent substitution $La^{3+}/Ba^{2+}$ has to modify the ionic charges and the effective interactions. The simplest way to model this perturbation is to apply the Cochran–Anderson model to $BaTiO_3$:La. In this model, the main contribution to the dielectric susceptibility arises from the zone centre transverse optical (TO) mode. As the ferroelectric transition temperature $T_0$ is reached from above the soft-mode frequency follows the equation [13]

$$\mu\omega_{TO}^2/F^* = A(T - T_0) \tag{1}$$

where $\mu$ is the reduced mass and $F^*$ is the effective Ti–O elastic interaction. This effective parameter includes the interionic Ti–O interaction and the intraionic deformation of the O ion, which is assumed to be the only polarizable ion.

In the ferroelectric axis direction, the optic mode splitting is [14]

$$\sum_j \left(\omega_{LO,j}^2 - \omega_{TO,j}^2\right)_\alpha = \frac{1}{\varepsilon_0 v}\sum_k \frac{Z_k^2}{m_k} \tag{2}$$

where $\omega_{LO}$ is the longitudinal optical mode frequency, $\varepsilon_0$ the free space dielectric susceptibility, $v$ the unit cell volume, $Z_k$ the ionic charge and $m_k$ the ionic mass. The index $k$ runs over the unit cell ions and $\alpha$ are the three spatial directions. In the cubic phase, the $j$ summation on the left hand side of equation (2) can be restricted to the ferroelectric soft $F_{1u}$ mode. In fact, the TO–LO mode splitting is negligible for all the other symmetries (see table 2).

**Table 2.** Mode splitting in the cubic phase of $BaTiO_3$. TO and LO stand for transverse optical and longitudinal optical modes respectively. Note that, in the cubic phase, only the lowest-frequency $F_{1u}$ mode displays a noticeable splitting, the other splittings being negligible. The data are given as frequencies in terahertz.

| | $F_{1u}$ | | $F_{1u}$ | | $F_{1u}$ | | |
|---|---|---|---|---|---|---|---|
| | TO | LO | TO | LO | TO | LO | $F_{2u}$ |
| IR [15] | 1.8 | 21.3 | 5.4 | 5.46 | 14 | 14.5 | × |
| Neutrons [16] | — | 21 | 5.4 | 5.4 | 15.5 | 15.5 | 9 |

Using the Lyddane–Sachs–Teller (LST) equation $(\varepsilon_s/\varepsilon_\infty) = (\omega_{LO}/\omega_{TO})_{q=0}^2$ and equation (1), equation (2) may be applied to $BaTiO_3$:La:

$$\varepsilon_s = \varepsilon_\infty\left[1 + \frac{1}{\varepsilon_0 v B F^*(T - T_0)}\left(\frac{(1-x)Z_{Ba^{2+}}^2}{m_{Ba}} + \frac{xZ_{La^{3+}}^2}{m_{La}} + \frac{(1-x)Z_{Ti^{4+}}^2}{m_{Ti}} + \frac{xZ_{Ti^{3+}}^2}{m_{Ti}} + 3\frac{Z_{O^{2-}}^2}{m_O}\right)\right]. \tag{3}$$

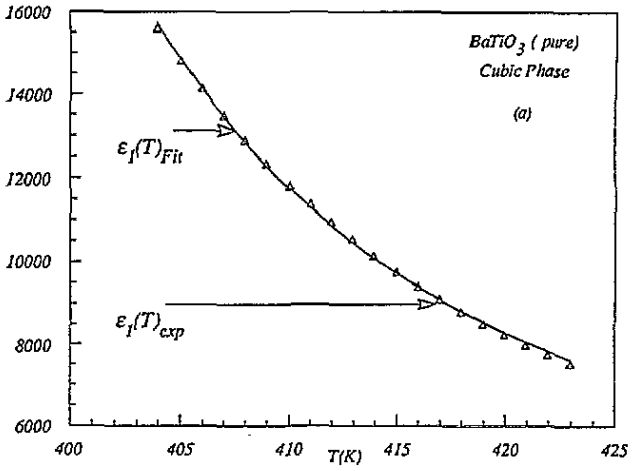


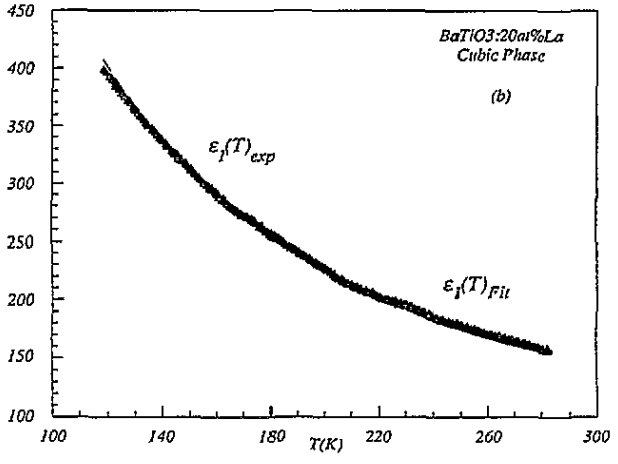


**Figure 8.** The real part of the dielectric susceptibility versus temperature in the cubic phase of $BaTiO_3$ (a) and $BaTiO_3$:La, 20 at.% La (b). The full lines are the Cochran–Anderson fit to the data (equation (3)).

The main assumption of equation (3) is that the only compensation of the heterovalent $La^{3+}/Ba^{2+}$ substitution is an ionization of $Ti^{4+}$ to $Ti^{3+}$.

We have used equation (3) to fit our dielectric data with five adjustable parameters: $\varepsilon_\infty$, $F^*$, $B$, $T_0$ and $Z(O)$. $\varepsilon_\infty$ is the optical contribution to the static susceptibility; $B$ and $T_0$ are the Curie parameters of the ferroelectric transition. The other ionic charges were set to the nominal values: $Z_{Ti^{4+}} = 4$, $Z_{Ti^{3+}} = 3$ and $Z_{La^{3+}} = 3$. The ionic charge of $Ba^{2+}$ will vary in order to keep the unit cell neutral.

Some of the resulting fits are given in figure 8 for pure and doped samples ($x_{La} =$ 20 at.%). We now discuss the evolution of the main fitting parameters $Z(O)$ and $F^*$ as a function of $x_{La}$. For high $La^{3+}$ content $x_{La} > 2\%$, the effective O charge is very high: $Z(O) > -1.5$. Due to the lack of microscopic data on the electronic O shells, this result cannot be discussed further. However, for $x_{La} < 2\%$, a clear maximum of $F^*$ is evidenced

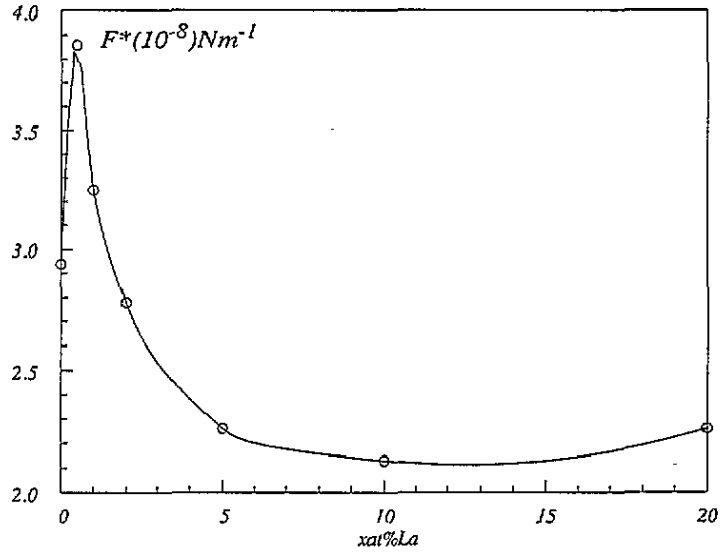


**Figure 9.** The effective Ti–O elastic interaction parameter versus La content. This parameter is the result of the best fits as given in figure 8.

(figure 9).

As a result, we point out that the effective elastic interaction displays an extremum behaviour in the same concentration range where the electric properties are optimal: 0.5 at.% $< x_{La} <$ 1 at.% (figures 6 and 9). The common origin of these two optimizations could be found in the charge transfer between the O anions and the adjacent $Ti^{4+}$ cations. This charge transfer is related to the substitution $La^{3+}/Ba^{2+}$. The charge compensation of this heterovalent process is either a creation of Ba vacancies or an ionization of the Ti ions.

An extremum behaviour of the lattice softening and of the conductivity is found for 0.5 at.% $< x_{La} <$ 1 at.%, which is the crossover range between the two above-mentioned compensating regimes.

Within this model it is thus possible to find a link between the lattice dynamics and the conductivity of $BaTiO_3$:La. This implies that the classical models for the PTCR property of this compound should be partly reconsidered.

## References

[1] MacChesney J P and Potter J F 1965 *J. Am. Ceram. Soc.* **48** 81
[2] Heywang W 1971 *J. Mater. Sci.* **6** 1214
[3] Kleint C A, Stöpel U and Rost A 1989 *Phys. Status Solidi* **115** 165
[4] Yamamoto T, Hideji I and Kiyoshi O 1983 *J. Am. Ceram. Soc.* **66** 363
[5] Batllo F 1987 *Thesis* Dijon
[6] Ching-Jui T, Cheng-Jieu P, Hong-Yang L and Shinn-Tyan W 1990 *J. Am. Ceram. Soc.* **73** 329
[7] Daniels J and Hardtl K H 1976 *Philips Res. Rep.* **31** 489–504
[8] Dhalenne G, Revcolevschi A and Collongues R 1972 *Mater. Res. Bull.* **7** 633
[9] Kiutty T R N, Murugara P and Gabhidje N S 1984 *Mater. Lett.* **2** 396
[10] Danilyuk Y L and Khartonou E V 1936 *Phys.–Solid State* **6** 260
[11] Possenriede E, Schirmer O F, Albers J and Godefroy G 1990 *Ferroelectrics* **107** 313
[12] Lahlafi A, Godefroy G, Ormancey G and Jullien P J 1993 *J. Opt. Soc. Am.* B **10** 1276

Schunemann P G, Temple D A, Hathcock R S, Tuller H L, Jenssen H P and Warde C 1988 *J. Opt. Soc. Am.* B 5 1685
[13] Cochran W 1961 *Adv. Phys.* **10** 401
[14] Scott J F 1970 *Phys. Rev.* B 4 1360
[15] Servoin J L 1980 *Thesis* Orléans
[16] Jannot B, Bouillot J and Escribe C 1984 *J. Phys. C: Solid State Phys.* **17** 1329